Finite Element Modelling of Plain and Reinforced Concrete Specimens with the Kotsovos and Pavlovic Material Model, Smeared Crack Approach and Fine Meshes

George Markou[1*] and Wynand Roeloffze[1†]

[1]Department of Civil Engineering, University of Pretoria, South Africa

[*]e-mail: george.markou@up.ac.za

[†]e-mail: u14090466@tuks.co.za

ABSTRACT

Modelling of concrete through 3D constitutive material models is a challenging subject due to the numerous nonlinearities that occur during the monotonic and cyclic analysis of reinforced concrete structures. Additionally, the ultimate limit state modelling of plain concrete can lead to numerical instabilities given the lack of steel rebars that usually provide with the required tensile strength inducing numerical stability that is required during the nonlinear solution procedure. One of the commonly used 3D concrete material models is that of the Kotsovos and Pavlovic, which until recently it was believed that when integrated with the smeared crack approach, it can only be used in combination with relatively larger in size finite elements. The objective of this study is to investigate into this misconception by developing different numerical models that foresee the use of fine meshes to simulate plain concrete and reinforced concrete specimens. For the needs of this research work, additional experiments were performed on cylindrical high strength concrete specimens that were used for additional validation purposes, whereas results on a reinforced concrete beam found in the international literature were used as well. A discussion on the numerical findings will be presented herein by comparing the different experimental data with the numerically predicted mechanical response of the under study concrete material model.

Keywords: Finite Element Method, Fine Meshes, Reinforced Concrete, High-Strength Concrete, Smeared Crack Approach, Damage Mechanics.

1. Introduction

Modelling concrete has been the subject of numerous research studies the last 70 years. The main approach foresaw the use of simplistic 1 or 2 dimensional material models that did not consider the full stress-strain relationship, leading towards non-objective numerical models that were able to capture specific behaviours of simple structural members such as beams and columns that are bending dominated. It was not until the last two decades that scientists began to investigate the option of modelling the concrete domain through a more detailed approach

that foresaw the use of 3D constitutive material models that have the ability to capture material nonlinearities due to micro-cracking and macro-cracking.

One of the most promising numerical models that were presented in the international literature was that of the Kotsovos and Pavlovic [1] in 1995 that was thereafter algorithmically improved by Markou and Papadrakakis [2]. The main objective of the work presented in [2], was to use this constitutive material to model full-scale structures through coarse meshes that would allow the seismic assessment of reinforced concrete (RC) structural systems under ultimate limit state conditions. An attempt of modeling full-scale structures was also presented by Engen et al. [3] in 2017, where large-scale models were analysed under monotonic loading conditions. The assumption in the prementioned research works was to use a 15-25 cm in size hexahedral elements for the discretization of the concrete domain.

Further development and use of the 3D detailed modeling approach was presented in [4-24], where the adoption of relatively large hexahedral elements was assumed. This assumption was solely based on computational restrictions and was not related to the fact that the proposed method was not suitable when finer meshes were used. One of the largest models that were nonlinearly analysed through the proposed modeling approach in [2] to date, is the RC bridge of 100m span presented in [25], which foresaw the use of more than 100,000 concrete hexahedral elements and more than half a million embedded rebars. The largest model to date is the Nuclear Building presented in [18] that foresaw the use of more than 2.7 million embedded rebar elements found within the 181,076 hexahedral concrete elements.

In order to investigate the mesh sensitivity of the method, a parametric investigation was performed in [2], where three different mesh sizes were used to discretize RC beams with and without stirrups. Nonetheless, the hexahedral elements did not foresee the use of fine meshes due to the corresponding modelling objective that foresaw the use of the 3D detailed modelling approach in full-scale RC structures analyses. A more recent attempt to investigate the mesh sensitivity of the method was performed by Markou and AlHamaydeh [26] in 2018, where the discretization of a deep beam reinforced with FRP-(fibre reinforced polymer) rebars was performed through the use of different in size hexahedral 20-noded elements. The smallest in size element that was used in that research work [26] was 5 cm, while the largest was 20 cm. According to the numerical investigation and the mesh sensitivity analysis it was demonstrated that the numerical results and the proposed method [26] were not significantly affected from the element size.

When using 3D concrete material models that are based on plasticity and a more homogenous approach in simulating cracking through continuum mechanics, the need of finer meshes is needed to achieve stable solutions. This observation was also confirmed by other researchers [27] where a comparison of the software packages ABAQUS [28], ANSYS [29] and LS-DYNA [30] was presented. Cotsovos et al. [30] had to use very small in size elements (1-3cm hexahedral edge size) to be able to proceed with the nonlinear analysis of a RC beam. When larger in size elements were used, the analysis was not able to provide with a complete P-δ

curve according to the results that were obtained when finer meshes were used [27]. Abed et al. [31] reported similar findings, where half of a RC deep beam was modelled due to the computational demand that derived from the adopted fine mesh that was developed in ABAQUS. Other research work that uses the concept of large sized elements and the Kotsovos and Pavlovic material can be found in [40, 41]. It is important to note at this point that, different material models were presented that aim to provide with mesh depended concrete material formulations [42-44], but will not be investigated in this research work given that this is outside of the research objectives of this manuscript.

Therefore, this research work has as a main objective to investigate the numerical response of the 3D model of Kotsovos and Pavlovic [1] as it was modified by Markou and Papadrakakis [2] and its ability to reproduce experimental data of normal and high strength concrete (HSC) specimens through the use of fine meshes. Furthermore, the ability of the proposed modelling approach [2] to reproduce experimental data of RC specimens when fine meshes are used, is also investigated in an attempt to conclude on whether the idea that the Kotsovos and Pavlovic constitutive concrete material model is only suitable for coarser meshes as stated in [1]. It is important to note at this point that the authors of [1] claim that due to the fact that the model was developed through the use of experimental data performed on concrete specimens that had dimension between 10-20 cm the numerical application of the constructed model is limited to hexahedral finite elements of this size. The research work presented in this manuscript will demonstrate that this is not true.

2. Experimental Campaign of High Strength Concrete

The numerical investigation aims to present the ability of the proposed modelling approach to capture both the standard and HSC specimens' mechanical response through fine meshes. Given that the modeling of standard plain concrete with fine meshes has been presented in [32] through the use of experimental data found in the international literature, experimental tests were performed on HSC cylindrical specimens to generate a sufficient number of experimental data to be used for the needs of the parametric investigation that will be presented in Section 4 on HSC as well.

HSC is a concrete that usually exceeds strength of 50 MPa 28 days [33] after casting. The strength of the concrete after 28 days of curing depends on the mix design and the admixtures and/or accelerators that have been added to the mix. Portland cements are commonly used for all concrete mixes not only in South Africa, but all over the world. It is important to know what these cements consist of to determine the properties the concrete mix will possess after a specific time. Table 1 is a table that explains the different types of Portland cements and the percentage of additions to the cement ingredients according to SANS 50197-1 [34], the design code used herein to develop the HSC mix.

In this study, a 52.5R cement [34] was used due to its rapid settling and its early strength after a few days. In terms of aggregates, dolomite rock was available to use at the laboratory, which

is a material that has the highest specific gravity for rocks available for concrete casting in South Africa. The quantities that were used to develop the HSC material are given in Table 2.

It was decided that 150 mm in diameter and 300 mm in height cylinders (see Fig. 1) would be used for the experiments. According to the experimental campaign, the cylinders were tested for four different curing durations (3, 7, 10 & 28 days). Young modulus values and compression strength tests were performed for all days of testing.

Table 1. SANS Classification of cement (SANS 50197-01)

Main Types	Notation of products (types of common cements)		Composition, percentage by mass										
			Clinker	Blastfurnace slag	Silica fume	Pozzolana		Fly ash		Burnt shale	Limestone		Minor additional constituents
						Natural	Natural calcined	Siliceous	Calcareous				
			K	S	D(b)	P	Q	V	W	T	L	LL	
CEM I	Portland cement	CEM I	95-100	-	-	-	-	-	-	-	-	-	0-5
CEM II	Portland-slag cement	CEM II A-S	80-94	6-20	-	-	-	-	-	-	-	-	0-5
		CEM II B-S	65-72	21-35	-	-	-	-	-	-	-	-	0-5
	Portland-silica fume cement Portland-pozzolanic cement Portland-fly ash cement Portland-burnt shale cement Portland-limestone cement	CEM II A-D	90-94	-	6-10	-	-	-	-	-	-	-	0-5
		CEM II A-P	80-94	-	-	6-20	-	-	-	-	-	-	0-5
		CEM II B-P	65-79	-	-	21-35	-	-	-	-	-	-	0-5
		CEM II A-Q	80-94	-	-	-	6-20	-	-	-	-	-	0-5
		CEM II B-Q	65-79	-	-	-	21-35	-	-	-	-	-	0-5
		CEM II A-V	80-94	-	-	-	-	6-20	-	-	-	-	0-5
		CEM II B-V	65-79	-	-	-	-	21-35	-	-	-	-	0-5
		CEM II A-W	80-94	-	-	-	-	-	6-20	-	-	-	0-5
		CEM II B-W	65-79	-	-	-	-	-	21-35	-	-	-	0-5
		CEM II A-T	80-94	-	-	-	-	-	-	6-20	-	-	0-5
		CEM II B-T	65-79	-	-	-	-	-	-	21-35	-	-	0-5
		CEM II A-L	80-94	-	-	-	-	-	-	-	6-20	-	0-5
		CEM II B-L	65-79	-	-	-	-	-	-	-	21-35	-	0-5
		CEM II A-LL	80-94	-	-	-	-	-	-	-	-	6-20	0-5
		CEM II B-LL	65-79	-	-	-	-	-	-	-	-	21-35	0-5
	Portland-composite cement	CEM II A-M	80-94	<---------- 6-20 ---------->									0-5
		CEM II B-M	65-79	<---------- 21-35 ---------->									0-5
CEM III	Blastfurnace cement	CEM III A	35-64	36-65	-	-	-	-	-	-	-	-	0-5
		CEM III B	20-34	66-80	-	-	-	-	-	-	-	-	0-5
		CEM III C	5-19	81-95	-	-	-	-	-	-	-	-	0-5
CEM IV	Pozzolanic cement	CEM IV A	65-89		<------ 11-35 ----->					-	-	-	0-5
		CEM IV B	45-64		<------ 36-55 ----->					-	-	-	0-5
CEM V	Composite cement	CEM V A	40-64	18-30	-	<------ 18-30 ----->			-	-	-	-	0-5
		CEM V B	20-39	31-50	-	<------ 31-50 ----->			-	-	-	-	0-5

Table 2. Quantities for the concrete mix

Materials	Mass (in kg)
Water	24.45 (24.45*l*)
Cement	64.34
Dolomite	192.97
Crushed Dolomite sand	168.53
Super-plasticizer	2.45 (2.45*l*)

Fig. 2 shows the experimentally obtained average uniaxial compressive strength of the HSC cylindrical specimens (a total of 24 HSC cylindrical specimens were constructed; six specimens per age). According to the graph, the concrete mix developed a uniaxial compressive strength of 50 MPa after 3 days of curing, while the maximum uniaxial compressive strength was observed after 28 days of curing, where a 75.62 MPa strength was recorded. Furthermore, Fig. 3 shows the experimentally obtained average Young moduli (E-values) for each set of cylinders that were tested during the different testing days. The values found in Figs. 2 and 3 were the exact values used in the numerical models developed for the needs of the 3D simulations presented in Section 4. It must be stated herein that half of the cylinders were used to perform tensile tests

Figure 1. Demoulded HSC cylinders.

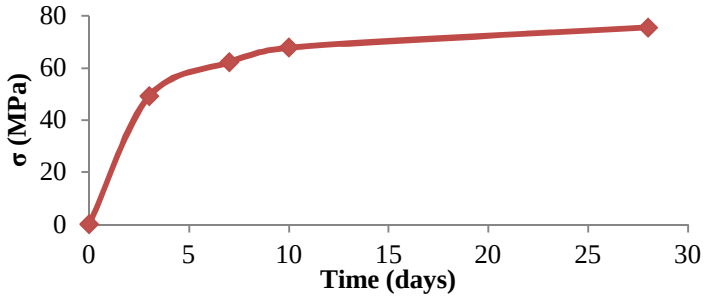

Figure 2. Graph of the average uniaxial compressive strength of the concrete cylinders over time

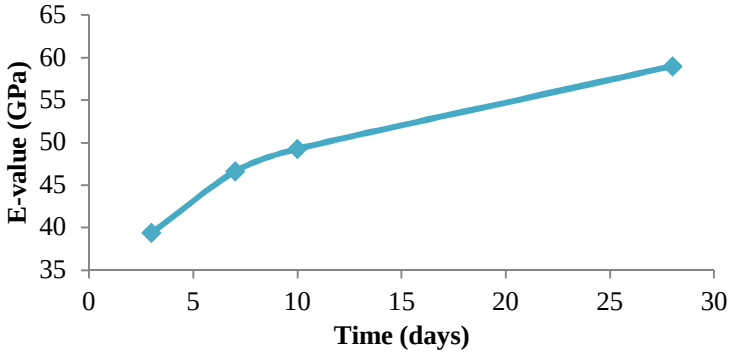

Figure 3. Average E-values of the HSC cylinders over time

3. Constitutive Material Modelling of Concrete and Steel Rebars

The concrete material model, as it was presented in [2], was developed by performing numerical regression on experimental data on concrete specimens that were tested under uniaxial and triaxial stress conditions [1]. The model foresees the use of generalized stress-strain relationships that are expressed by decomposing each state of stress into a hydrostatic (σ_0) and a deviatoric component (τ_0). According to the material model formulation, the hydrostatic and deviatoric stresses that are computed from the corresponding hydrostatic and deviatoric strains (ε_0, γ_0) are expressed as follows:

$$\varepsilon_0 = \varepsilon_{0h} + \varepsilon_{0d} = \frac{\sigma_0 + \sigma_{id}}{3K_S}, \qquad \gamma_0 = \frac{\tau_0}{2G_S} \tag{1}$$

In Eq. 1, $\sigma_{id}(\sigma_0,\tau_0,f_c)$ is the equivalent internal hydrostatic stress that accounts for the coupling between τ_0 and ε_{0d}. Furthermore, the secant bulk and shear moduli $K_S(\sigma_0,\tau_0)$ and $G_S(\sigma_0,\tau_0)$ are obtained by assuming that the coupling stress σ_{id} is ignored.

Given that the stress σ_{id} is a pure hydrostatic correction, the relationships in Eq. 1 are equivalent to:

$$\varepsilon_{ij} = \frac{\sigma_{ij} + \sigma_{id}\delta_{ij}}{2G_S} - \frac{3\nu_S}{E_S}\left(\sigma_0 + \sigma_{id}\right)\delta_{ij} \tag{2}$$

where, δ_{ij} is the Kronecker delta, σ_{ij} and ε_{ij} are the total stresses and strains, respectively. Eq. 2 is a relationship expressed in the Global coordinate system. $E_S(\sigma_0,\tau_0,f_c)$ and $\nu_S(\sigma_0,\tau_0,f_c)$ are the secant Young modulus and Poisson ratio, respectively, derived from K_S and G_S, using the standard expressions in Eq. 3.

$$E_S = \frac{9K_SG_S}{3K_S + G_S}, \qquad \nu_S = \frac{3K_S - 2G_S}{6K_S + 2G_S} \tag{3}$$

For determining whether concrete has failed, the Willam and Warnke [35] formula is used:

$$\tau_{0u} = \frac{2\tau_{0c}(\tau_{0c}^2 - \tau_{0e}^2)\cos\theta + \tau_{0c}(2\tau_{0e} - \tau_{0c})\sqrt{4(\tau_{0c}^2 - \tau_{0e}^2)\cos^2\theta + 5\tau_{0e}^2 - 4\tau_{0c}^2\tau_{0e}^2}}{4(\tau_{0c}^2 - \tau_{0e}^2)\cos^2\theta + (2\tau_{0e} - \tau_{0c})^2} \tag{4}$$

This expression describes a smooth convex curve that is graphically presented in Fig. 4. Within Eq. 4, θ represents the rotational angle that the deviatoric stress vector forms with one of the projected stress principal axes on the deviatoric plane. As it can be seen in Fig. 4, τ_{0e} and τ_{0c} are the deviatoric stresses that form at $\theta = 0^o$ and $\theta = 60^o$, respectively. Additionally, when the failure criterion is satisfied, the smeared crack approach is activated, where the macro-cracking is simulated accordingly [2].

It is also important to note here that the concrete material model was algorithmically improved as it was discussed in [2]. Following an extensive parametric investigation, it was found that in the case where the ultimate deviatoric stress τ_{0u} at a specific Gauss point was smaller than 50% of the ultimate strength expressed by Eq. 4, then the elastic constitutive matrix of that Gauss

point could be used during the stiffness matrix computation. For the case when the deviatoric stress τ_{0u} exceeded the 50% of the concrete ultimate strength, then the material law was used to update the constitutive matrix by updating the K_T and G_T tangential moduli. For more information, one may refer to [2] and [32], whereas the latest advances in nonlinear cyclic analysis of bare and retrofitted RC structures can be found in [19] and [22].

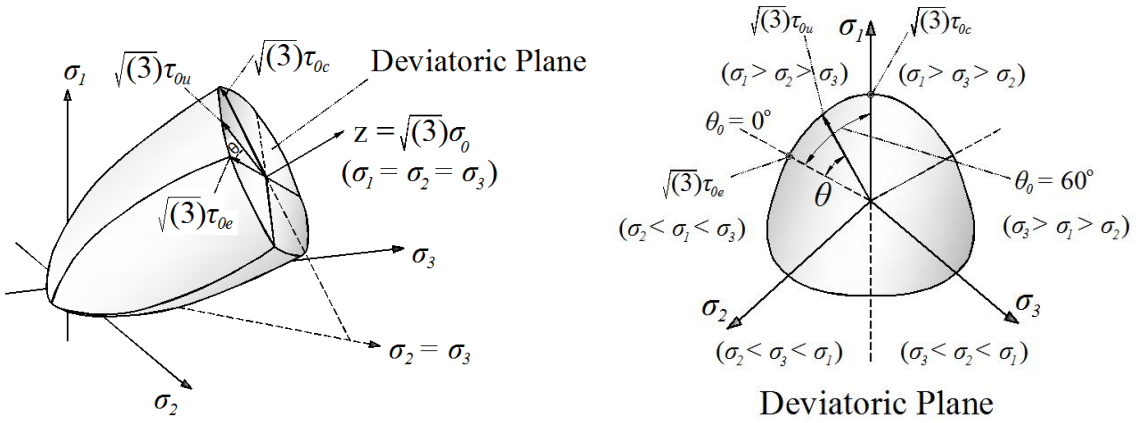

Figure 4. Graphical representation of the concrete's ultimate-strength surface. (a) 3D view in the stress space and (b) typical cross-section of the strength envelope that coincides with a deviatoric plane. [2]

In regards to modeling the embedded steel rebars, the material incorporated in Reconan FEA [36] which was the software used to perform all numerical analysis presented in this work, was that of Menegotto-Pinto [37] that also accounts for the Bauschinger effect. The steel material relationships of stress-strain take the following form:

$$\sigma^* = b\varepsilon^* + \frac{(1-b)\varepsilon^*}{(1+\varepsilon^{*R})^{1/R}} \tag{5}$$

where,

$$\varepsilon^* = (\varepsilon - \varepsilon_r)/(\varepsilon_0 - \varepsilon_r), \tag{6}$$

$$\sigma^* = (\sigma - \sigma_r)/(\sigma_0 - \sigma_r) \tag{7}$$

$$R = R_0 - a_1\xi/(\alpha_2 + \xi) \tag{8}$$

It must be noted at this point that b is the strain hardening ratio and ξ the normalized plastic strain variable. Furthermore, the parameters R_0, a_1 and a_2 were determined through numerical investigations and assumed herein to be equal to 20, 18.5 and 0.15, respectively.

4. Numerical Investigation

4.1 Normal Strength Concrete Specimens

As it was presented in [32], the experimental data found in [38] were used to test the abilities of the developed algorithm proposed in [2] in capturing the mechanical response of cylindrical specimens constructed out of normal strength concrete. Fig. 6a shows the experimental setup and the corresponding stress-strain curves that were used to validate the developed algorithm.

Specimen N2 was chosen for the validation procedure, a specimen that derived a maximum uniaxial strength of 40 MPa. The dimensions of the specimens [38] foresaw for a *10 cm* diameter and a *20 cm* height.

The specimen was discretized through the use of 8-noded isoparametric hexahedral elements with sizes of *1*, *2*, *3* and *10 cm* along their height (see Fig. 6). Additionally, the steel crushing plates were also discretized through the use of hexahedral elements that assumed a linear material behaviour (see red elements in Fig. 6). One of the main advantages of the material model proposed in [1] is that it requires the minimum number of material concrete properties to be defined prior to any analysis. These are the uniaxial compressive strength f_c, the Young modulus of elasticity E_c, the Poisson ratio v, the tensile strength f_t (which is usually a percentage ratio of the uniaxial compressive strength) and the shear remaining strength factor β along the crack plane. According to the experimental data found in [38], the uniaxial compressive strength of concrete was equal to 40 MPa (Specimen N2), where a 30 GPa Young modulus of elasticity was used in the numerical models.

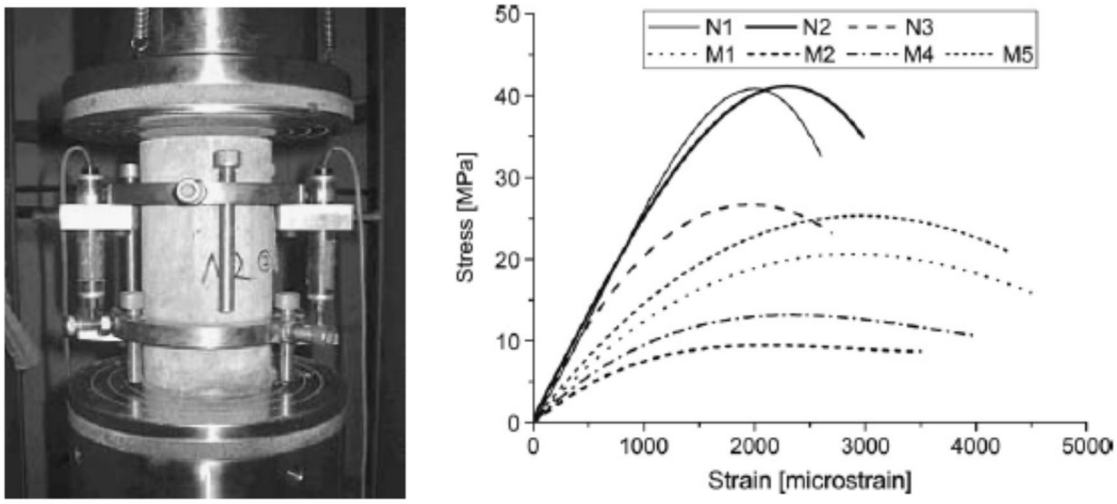

a. b.

Figure 5. (a) Uniaxial compressive test setup and (b) experimentally obtained stress-strain curves [38].

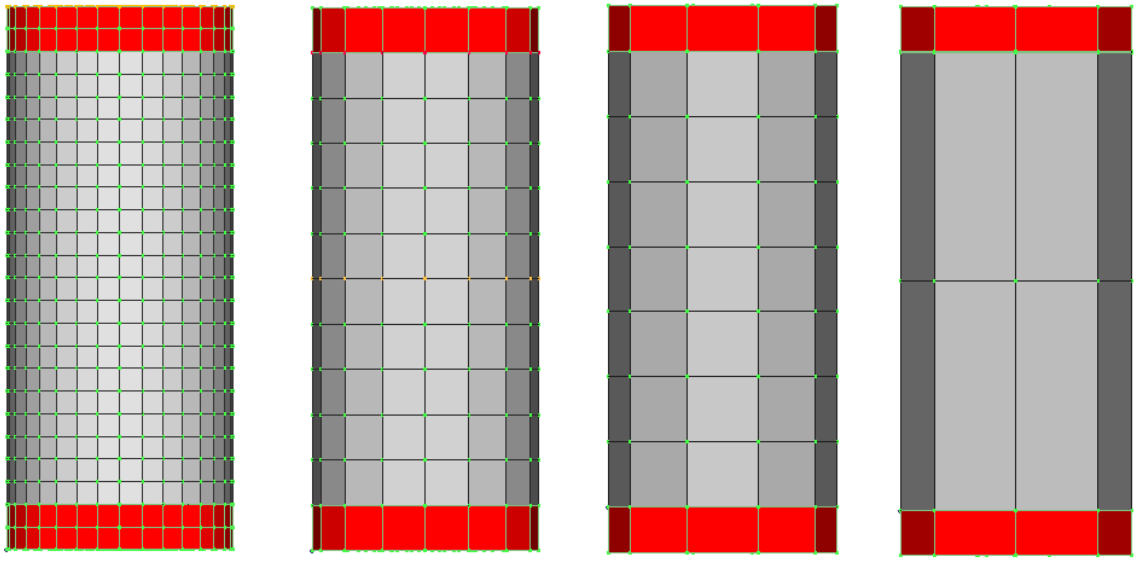

a. b. c. d.

Figure 6. Finite element hexahedral meshes. (a) 1, (b) 2, (c) 3 and (d) 10 cm height of each element layer.

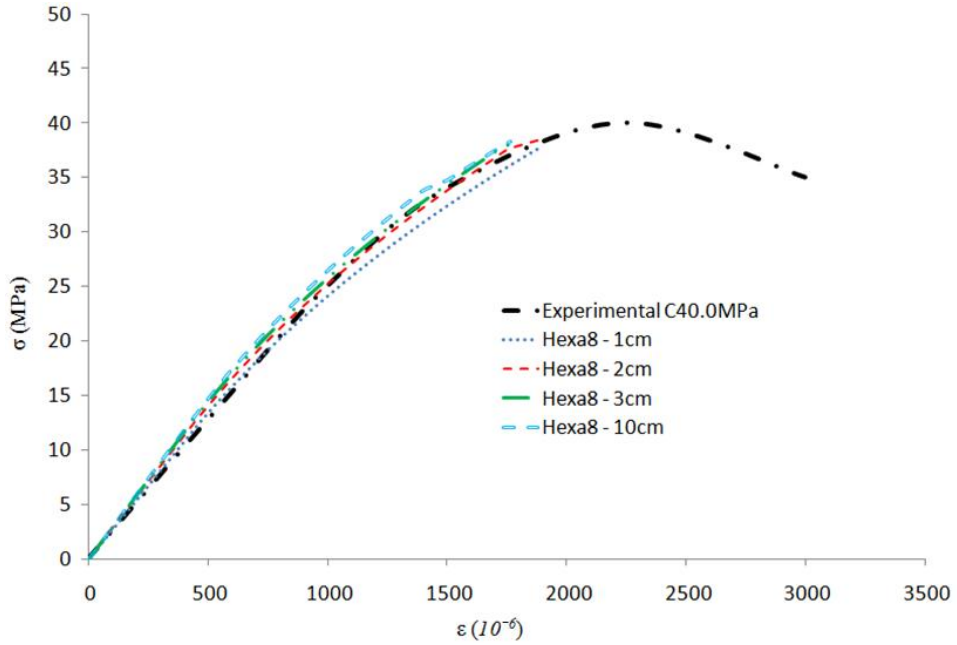

Figure 7. Normal strength concrete. Numerical vs experimental stress-strain results.

Fig. 7 shows the comparison between the experimental data and the numerically obtained stress-strain curves. It is indisputable that the modeling approach manages to capture the mechanical response of the specimen exhibiting an overall deviation of 5% from the experimental data in terms of ultimate failure stress. In addition, the element size is found to affect the flexibility of the models, a well know numerical phenomenon of the finite element method, but does not significantly affect the prediction abilities of the four numerical models. Before moving to the investigation of the HSC cylindrical specimens, the deformed shape of the 2 cm hexahedral element model is shown in Fig. 8, where it is easy to observe the ability of the solid elements to capture the lateral expansion of the cylindrical concrete specimen due to the compressive load. Additionally, the local confinement at the areas where the concrete specimen is connected to the steel plates is visible.

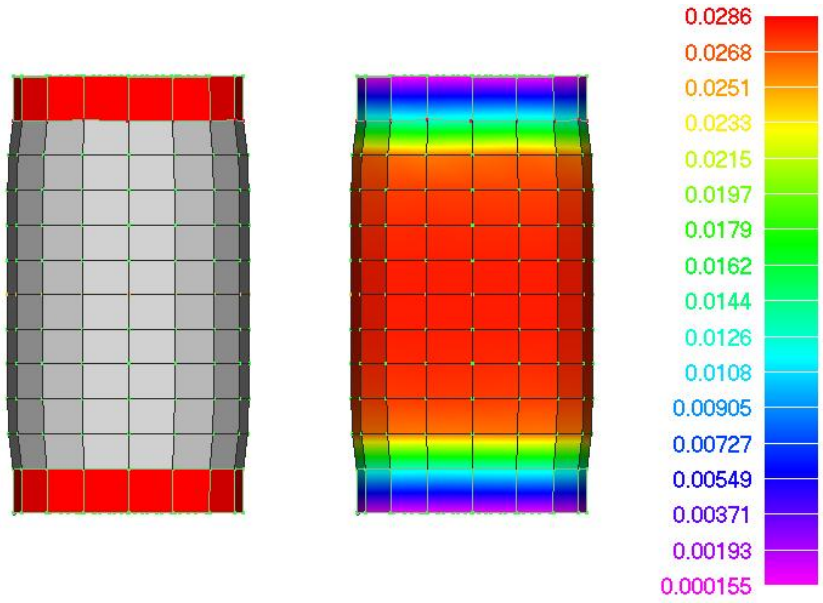

Figure 8. Normal strength concrete. Deformed shape prior to failure and von Mises strain contour. 2 cm hexahedral element size model.

To further investigate the numerical response of Reconan's nonlinear solvers (displacement- and force-control) when combined with the developed material model and fine meshes, the specimen in Fig. 5, was re-meshed by using a 2 and 3 cm element sizes. Given that the FE meshes shown in Fig. 6 were developed by auto meshing a cylinder of 10 cm diameter, the final polygon section's area of the mesh was around 6% smaller than the circular area of the physical specimen for the case of the 3 cm model and around 2.5% smaller for the 2 cm model. This was also the reason why the stress diagrams in Fig. 7 were not able to reach the ultimate compressive strength. Therefore, the newly developed meshes for the needs of this numerical investigation, foresaw a relevant increase of the cylindrical geometry that would thereafter auto meshed assuring that the total area of the elements along the *xy* plane would be equal to the area of a circular section of a 10 cm diameter.

Furthermore, the two new meshes were analysed by using both the force- and displacement-control solvers integrated within Reconan FEA, where two different displacement and load increments were assumed. As it can be seen in Fig. 9, the imposed displacement was set to 1 mm, while the displacement-control analysis was performed for two different total displacement increment steps, 50 and 100. The same number of load increments (50 and 100) were implemented for the force-control nonlinear analysis. This was performed to further investigate the robustness of the nonlinear solvers and the material model when combined with fine meshes.

Fig. 10a shows the numerically obtained stress-strain curves for the case of the force-control (FC) nonlinear analyses that foresaw 50 and 100 load increments. As it can be seen, the numerically obtained curves managed to capture the uniaxial compressive strength with an average accuracy of 3% (see Table 3), while the two models (2 and 3 cm meshes) managed to reproduce the experimental data in an almost identical manner. It is also easy to observe that

the same results derived from all the performed displacement-control (DC) analyses that also foresaw the implementation of the imposed displacement through 50 and 100 steps.

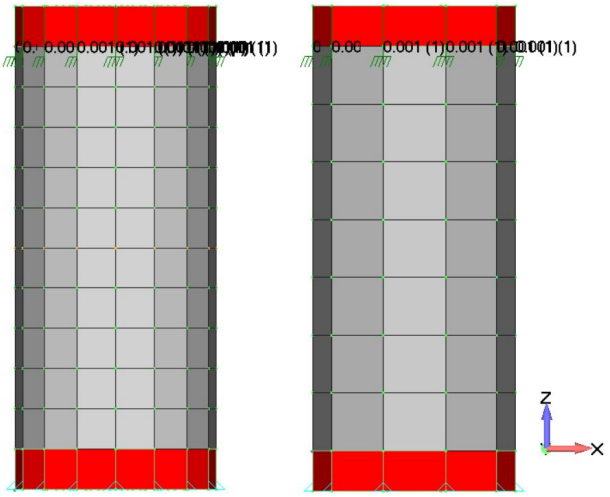

Figure 9. Normal strength concrete. Re-meshed cylindrical specimens with imposed displacements.

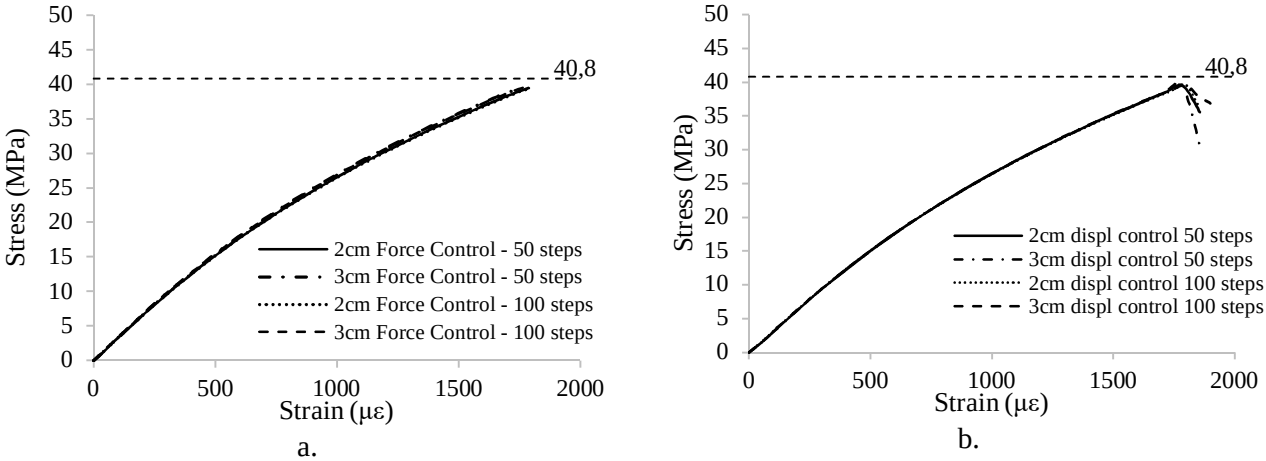

Figure 10. Normal strength concrete. Stress strain curves (a) Force- and (b) Displacement-control analyses with 50 and 100 increments.

Table 3. Experimental vs numerical ultimate uniaxial compressive strength.

Model	Max Strength f_{cu} (Mpa)	$\frac{f_{cu,exp}-f_{cu,num}}{f_{cu,exp}}$
Experiment	40.8	-
2cm FC - 50 steps	39.43	3.37%
2cm FC - 100 steps	39.43	3.37%
3cm FC - 50 steps	39.29	3.71%
3cm FC - 100 steps	39.73	2.62%
2cm DC - 50 steps	39.48	3.24%
2cm DC - 100 steps	39.59	2.98%
3cm DC - 50 steps	39.57	3.01%
3cm DC - 100 steps	39.61	2.92%
	Avg.	3.15%

Note: FC: Force-Control, DC: Displacement-Control

Table 3, shows the comparison between the experimentally obtained uniaxial compressive strength and the corresponding numerically derived concrete ultimate stress. It is evident that all the under study numerical models managed to capture the experimental data without any numerical instabilities, while the resulted stress-strain curves were not affected by the solver type (FC or DC). In addition to that, it is important to mention at this point that the nonlinear analysis was performed in a computationally efficient manner given that the largest model required a mere 3 seconds to be solved (2 cm model with 100 load/displacement increments). It is also important to state at this point that, the sudden loss of capacity observed within Figs. 7 and 10 is attributed to the brittle type of the concrete material model that assumes a total loss of strength along the perpendicular direction of the crack plane, after a macrocrack has occurred.

4.2 High Strength Concrete Specimens

All four HSC cylindrical specimen groups that were tested for the needs of this research work, were modelled and analysed through the use of two different models that foresaw a 2.5 cm and a 5 cm 8-noded hexahedral isoparametric finite element (FE) size, respectively. The two different meshes that were constructed and used in the parametric investigation presented in this section can be seen in Fig. 11. The approach used to develop the two meshes foresaw the construction of a cylindrical geometry that was then used to apply an automatic discretization attribute that assumed a 2.5 and 5 cm element size, respectively.

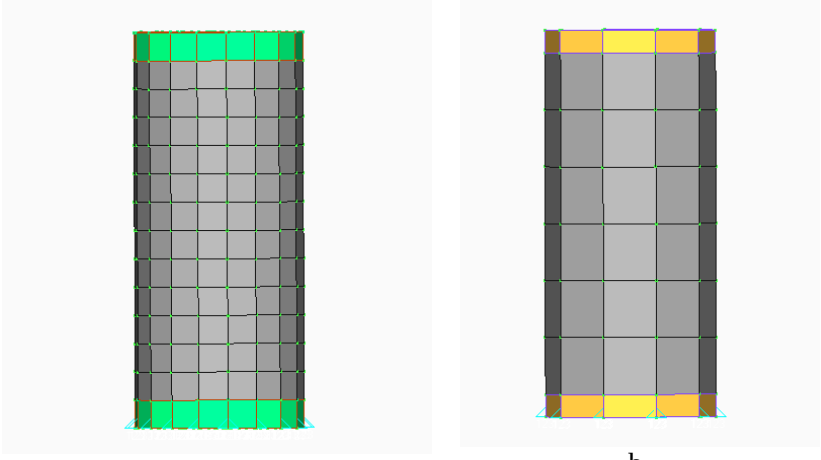

a. b.

Figure 11. HSC cylindrical specimens. (a) 2.5 cm and (b) 5 cm hexahedral meshes.

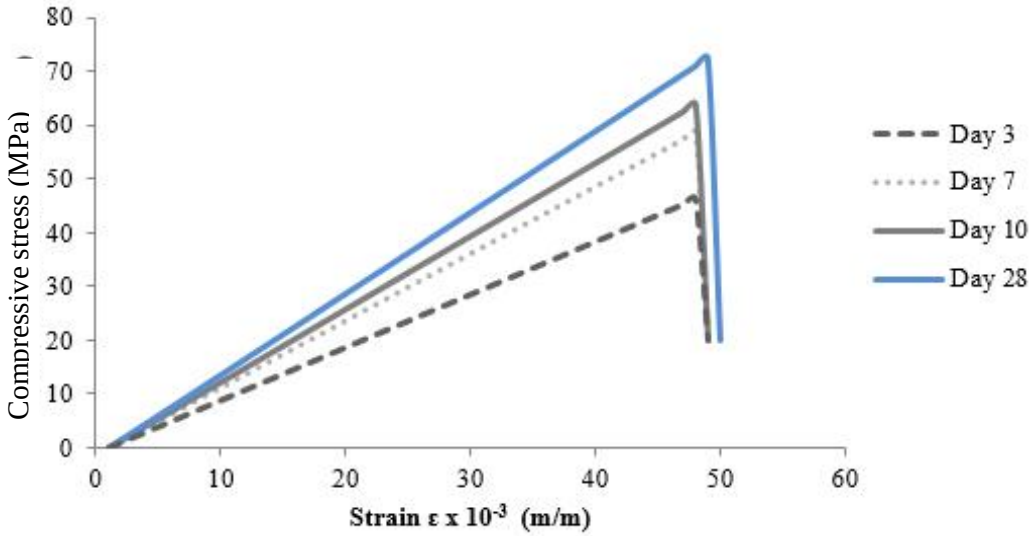

Figure 12. HSC cylindrical specimens. Stress vs strain curves of the 2.5 cm models.

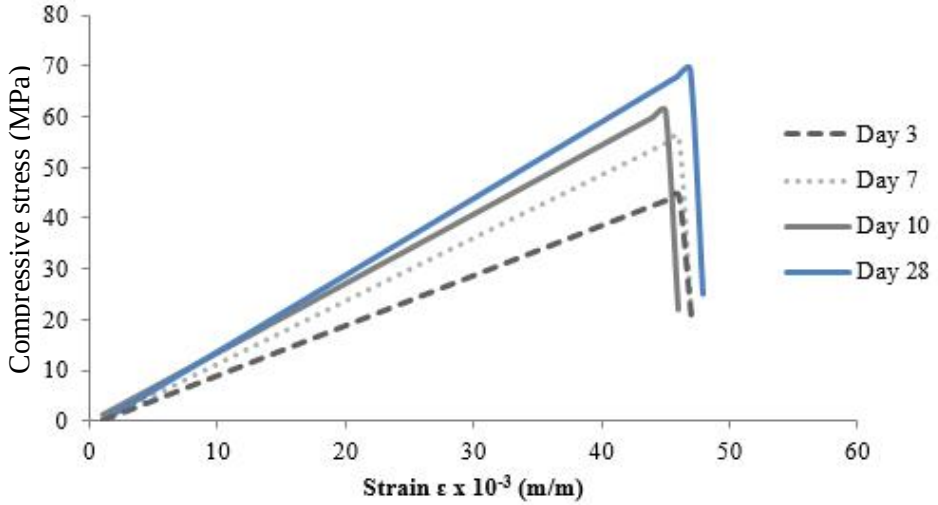

Figure 13. HSC cylindrical specimens. Stress vs strain curves of the 5 cm models.

Figs. 12 and 13 show the numerically obtained stress-strain curves as they resulted from the two models for the cases of the 3, 7, 10 and 28 days HSC specimens. It is easy to observe that the numerically predicted response of the HSC cylinders is characterised by a linear mechanical response that is followed by an abrupt loss of capacity due to macro-cracking. This mechanical behaviour is usual and attributed to the significant energy stored within the HSC specimens during the uniaxial compressive test, whereas, when the first macro-cracks occur they fail in an explosive manner. It is important to note that the vertical sudden drop at the end of each curve was artificially added so as to indicate the complete loss of strength at the point where the numerical models completely lost their carrying capacity.

Table 4 shows the comparison between the numerical predicted ultimate uniaxial strengths predicted from the two models for all four curing cases and the corresponding experimentally recorded data. It is evident that the numerical models managed to predict the uniaxial strength of all specimens with an overall deviation from the experimental data of less than 10%. The experimental results are compared with the numerically obtained ultimate strengths in Fig. 14 where the good agreement between them can be seen, while the numerical results were found

to be always in favour of safety. According to this graph (Fig. 14), it can be also depicted that the 5 cm models derived a smaller ultimate uniaxial strength compared to the 2.5 cm models. This numerical finding is attributed to the method through which the cylinders were discretized. As stated above, the method foresaw the use of 15 cm in diameter cylinder that was auto-meshed using the desired element size. This caused the 5 cm models to have a smaller volume compared to the 2.5 cm models that were better discretized given the smaller element size.

Table 4. HSC cylindrical specimens. Numerically and experimentally obtained ultimate uniaxial strength.

2.5 cm FE Model			
Day no.	**Experimental (MPa)**	**FE Model (MPa)**	**Difference (%)**
3	49.22	46.27	6.0
7	62.18	58.45	6.0
10	67.84	63.77	6.0
28	75.6	72.58	4.0
		Average	5.5

5 cm FE Model			
Day no.	**Experimental (MPa)**	**FE Model (MPa)**	**Difference (%)**
3	49.22	44.3	10.0
7	62.18	55.96	10.0
10	67.84	61.06	10.0
28	75.6	69.56	8.0
		Average	9.5

Figs. 15 and 16 show the deformed shapes and von Mises contours prior to failure, as they derived from the nonlinear numerical analysis. Furthermore, Fig. 17 compares the experimentally observed cracks with the numerically predicted crack pattern. It is clearly visible that the crack patterns form in the vertical direction due to the lateral tensile stresses that develop during the uniaxial compressive loading test, which complies with the experimentally observed crack patterns. The smeared crack approach smears the crack openings to the volume of concrete thus the numerically predicted cracks are denser compared to the actual crack patterns that resulted in the physical specimen. Nevertheless, the numerical model manages to capture the mechanical response of the HSC cylindrical specimens through fine mesh considerations without any numerical instabilities.

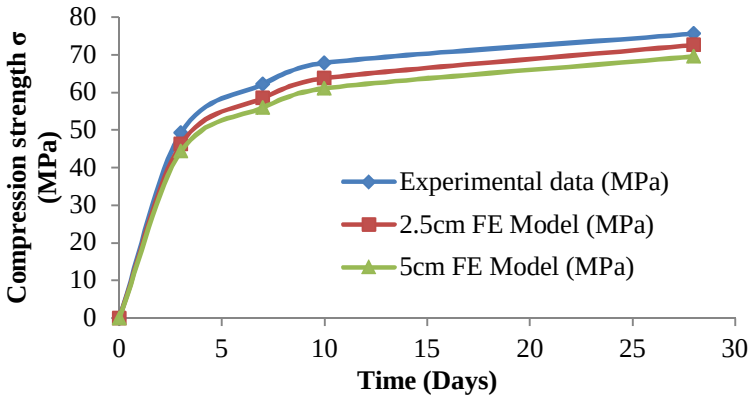

Figure 14. HSC cylindrical specimens. Numerical vs experimental data. Ultimate obtained compressive strength.

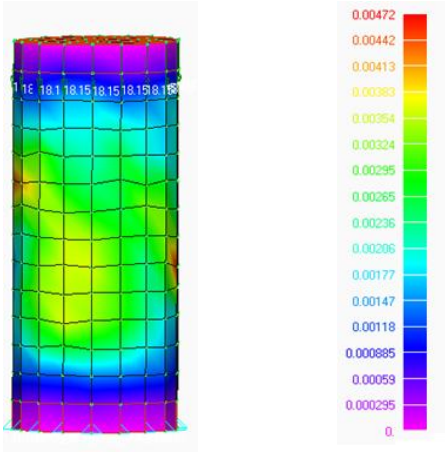

Figure 15. HSC cylinder with 2.5 cm elements. Deformed shape and von Mises strain contour prior to failure.

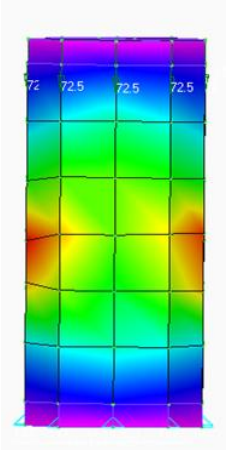

Figure 16. HSC cylinder with 5 cm elements. Deformed shape and von Mises strain contour prior to failure.

4.3 Reinforced Concrete Beam

A final model was developed in order to investigate the ability of the proposed numerical method [2] to reproduce experimental results or RC structural members through the use of fine meshes. To investigate the numerical response of the developed algorithm in this instance, a RC beam that was tested under a four-point bending test [39] is finely discretized and analysed in this section. The RC beam was reinforced with 12 mm in diameter tensile steel rebars and 5.6 mm in diameter compressive longitudinal reinforcement. According to [39], the shear reinforcement that was used to strengthen the 2 m long beam (1.8 m net span) also foresaw the use of 5.6 mm in diameter steel rebars spaced at 10 cm. The RC beam had a section of 15x23 cm, where a general concrete cover of 2 cm was used.

a. b.

Figure 17. HSC cylindrical specimens. (a) Experimentally observed crack pattern after failure and (c) crack pattern prior to failure according to the numerical model.

The RC beam was simply supported and was tested under a four-point bending configuration (two concentrated loads were applied at a 60 cm distance from each support). After concrete casting, the beam was cured for 7 days, where the actual testing took place. The reported material properties [39] for concrete that were also defined within the developed numerical model discussed in this section, foresaw a 37.2 MPa uniaxial compressive strength, a 3.03 MPa tensile strength and a 34.9 GPa Young modulus of elasticity. Tensile tests were also performed to acquire the material properties of the two different in diameter rebars that were used to reinforce the RC beam specimen. The steel modulus of elasticity was measured as 215.9 GPa and 221.4 GPa for the 12 mm and 5.6 mm in diameter reinforcement, respectively. Finally, the yielding stress was a theoretical value of 450 MPa for both rebar diameters, but was not experimentally measured in [39]. The ultimate strain for steel was set to be equal to 15%.

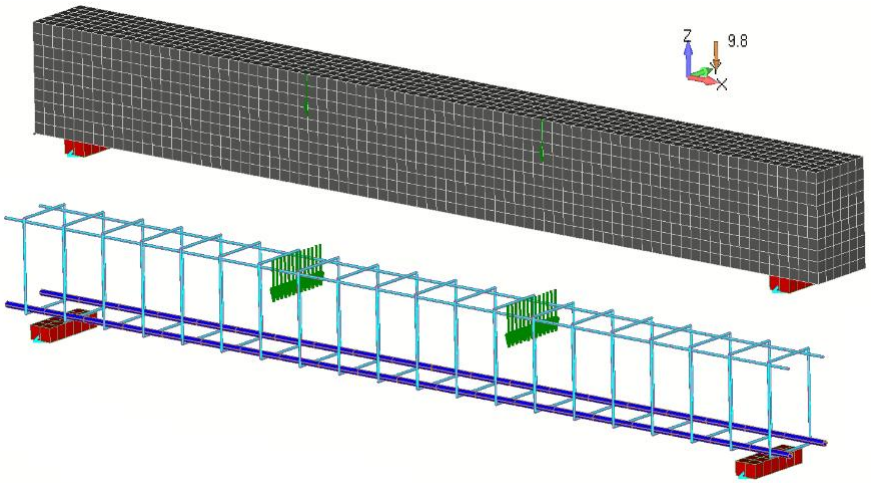

Figure 18. RC beam. Hexahedral and embedder rebar element mesh. 25 mm hexahedral edge size.

In order to develop the FE mesh for the nonlinear vertical push over analysis, a 2.5 cm size 20-noded hexahedral element was used. The computational demand of the 20-noded hexahedral element is significantly higher than that of the 8-noded element, thus it was adopted herein to further investigate the ability of the developed algorithm in capturing the mechanical response

of RC structural members through the use of computationally demanding problems. Fig. 18 shows the mesh that was developed through the use of the 2.5 cm hexahedral element, where the reinforcement was discretized with the embedded rod element. The model foresees the use of 4,800 concrete hexahedral elements, 24 steel hexahedral elements that were used to discretize the steel plates found at the supports and 960 embedded rebar rod element for simulating the reinforcement.

Fig. 19 shows the numerically obtained curves as they derived from the nonlinear analysis. The curves were developed by using three different load increments during the force-control analyses that foresaw the division of the total applied load into 10, 50 and 100 increments, respectively. It is easy to observe that the differences between the three numerically derived curves are negligible and attributed to the different load increment steps assumed during the three nonlinear analyses. It is also easy to observe that the numerical curves are in a good agreement with the experimental data, where the ultimate failure load was predicted with an average 4.4% deviation from the experimental value. Table 5 shows the comparison between the numerically predicted ultimate forces and the experimental failure load. It is also easy to observe that the physical specimen did not derive an elastic branch that is attributed to the fact that the RC beam had developed small cracks due to an initial loading applied to the specimen prior to the test [39]. Furthermore, Fig. 19 shows that the first cracking occurred at a total applied load of 11.5 kN according to the 50 and 100 load increment models. Given that the two nonlinear analyses that foresaw 50 and 100 load increments derived almost identical results, the 10 and 50 load increments will be further discussed herein.

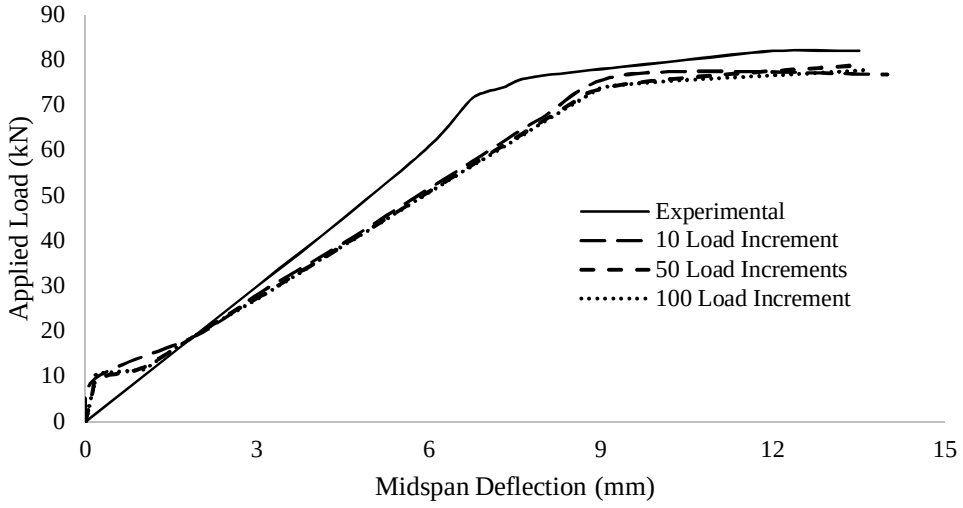

Figure 19. RC beam. Experimental vs numerical P-δ curves.

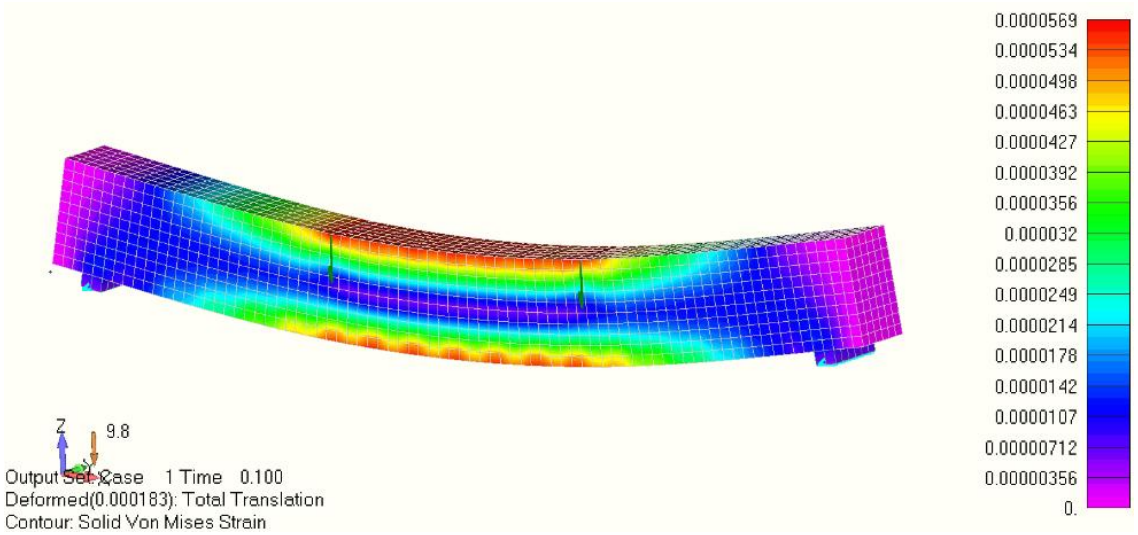

Figure 20. RC beam. Von Mises strain contour. Load step 1 prior to first crack opening. 10 load increments.

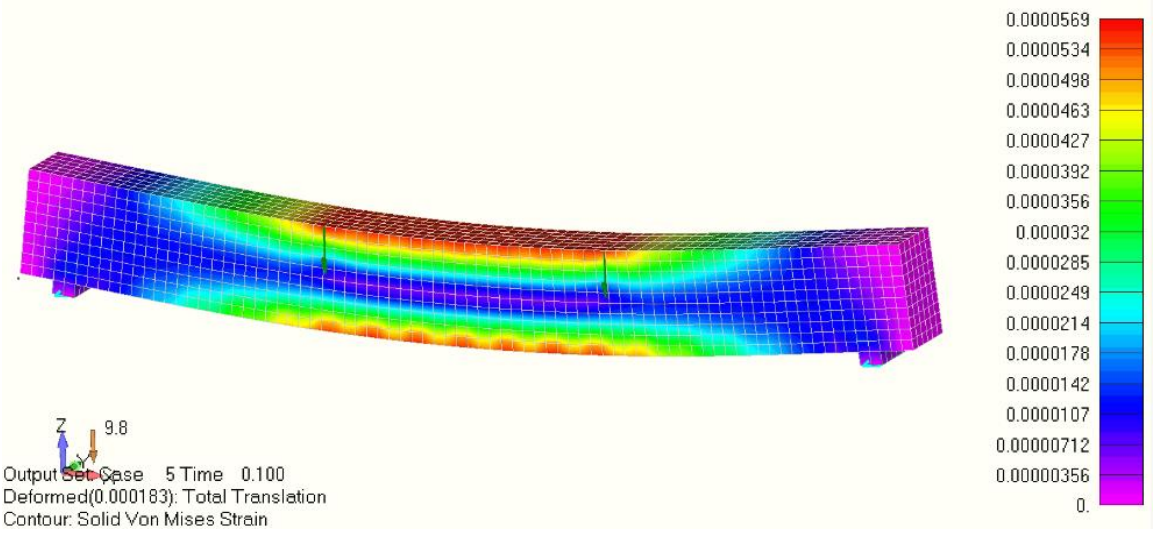

Figure 21. RC beam. Von Mises strain contour. Load step 5 prior to first crack opening. 50 load increments.

Table 5. Numerical vs experimental ultimate failure load.

a/a	Model	Ultimate load from analysis F_{num} (kN)	Difference from experimental
1	Experiment F_{exp}	82.00	-
2	10 load increments	76.80	6.3%
3	50 load increments	80.64	1.7%
4	100 load increments	77.76	5.2%

Figs. 20 and 21 show the von Mises strain contours prior to failure for the 10 and 50 load increment models, respectively. According to analysis, the two models managed to compute the exact same strain contour, thus reproduce the exact same deformed shape at the structural level independently to the load increment size. Thereafter, the first damages occurred within the concrete domain due to the opening of tensile cracks that appear at the midspan of the RC beam. The corresponding von Mises strain contours at the first crack openings that derived from the two analyses can be seen in Figs. 22 and 23 for the 10 and 50 load increment models,

respectively. It is evident that the first model that assumes larger load increments (step 2; total applied load of 19.2 kN) derives higher strain concentrations in comparison to the second model that predicts a more accurate first crack opening load step (total applied load 11.5 kN; step 6) due to the smaller load increment assumed. This numerical finding is well known when nonlinear analysis is performed through the use of the FE method, while the nonlinear solver that was used to perform the analysis is characterized by numerical stability and robustness.

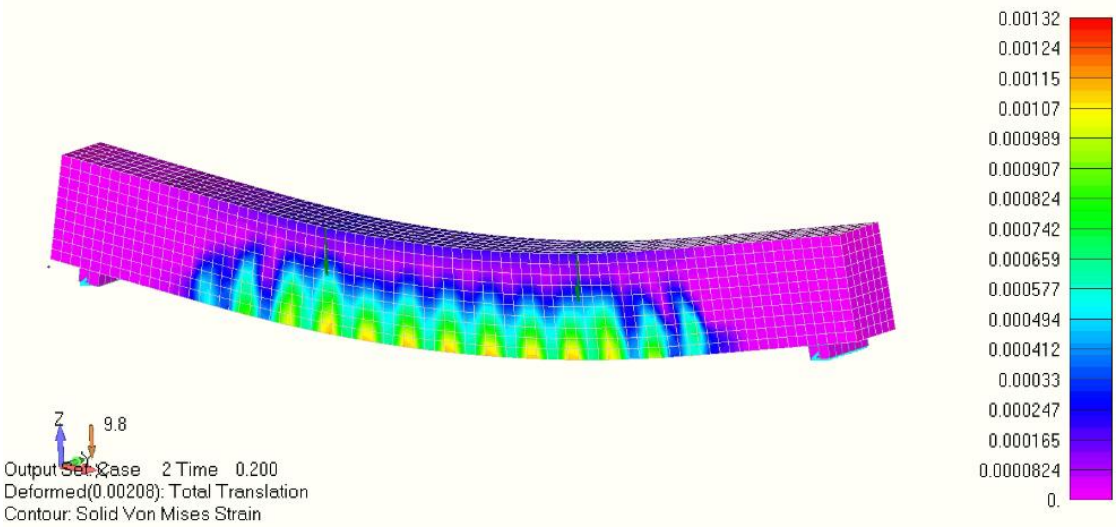

Figure 22. RC beam. Von Mises strain contour. Load step 2 - First crack opening. 10 load increments.

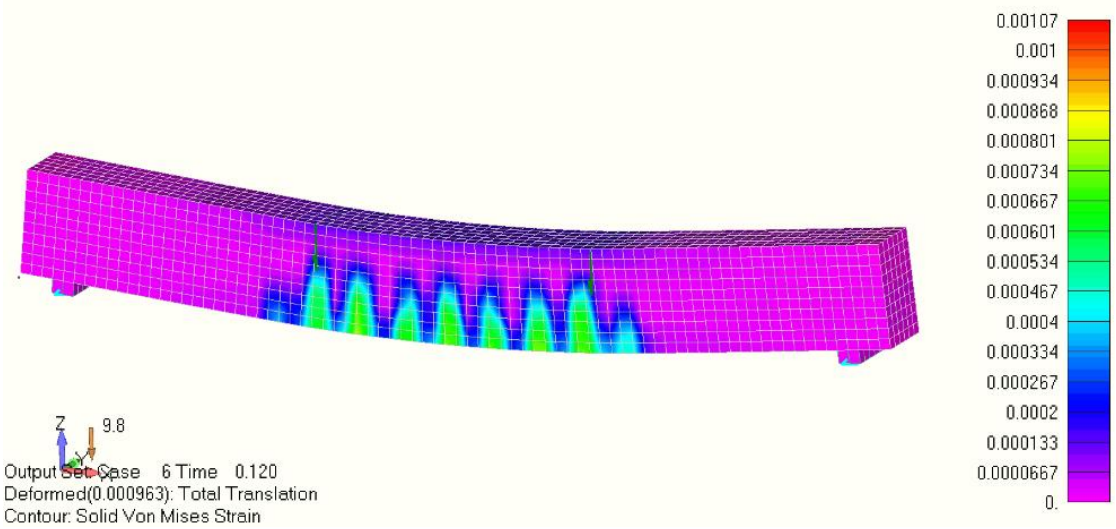

Figure 23. RC beam. Von Mises strain contour. Load step 6 - First crack opening. 50 load increments.

Finally, the von Mises strain contour prior to failure according to the two analyses is given in Figs. 24 and 25, where the maximum computed strains were 1.66%. In order to better visualize the strain contours the legend's maximum strain was capped in both figures to 0.5%, hence the areas that are red in colour represent strains equal or larger than 0.5%. Half of the concrete domain is visualized, where the embedded rebars and their deformed shape can be also seen. The differences in terms of strain contours are attributed to the different load level for which they are visualized. In this case, the 10-load increment model managed to converge during step 8 (total applied load of 76.8 kN) and failed after load increment 9 was implemented. On the

other hand, the second model managed to compute a balance point for a total applied load of 78.72 kN (step 41), while it failed to converge due to a rebar tensile failure at load step 42.

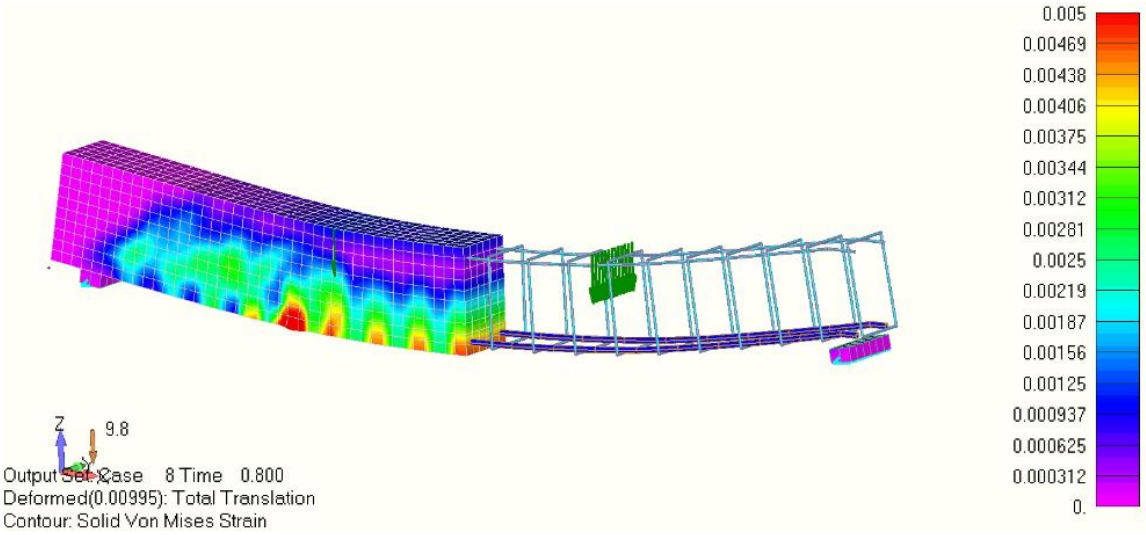

Figure 24. RC beam. Von Mises strain contour and deformed shape prior to failure. 10 load increments.

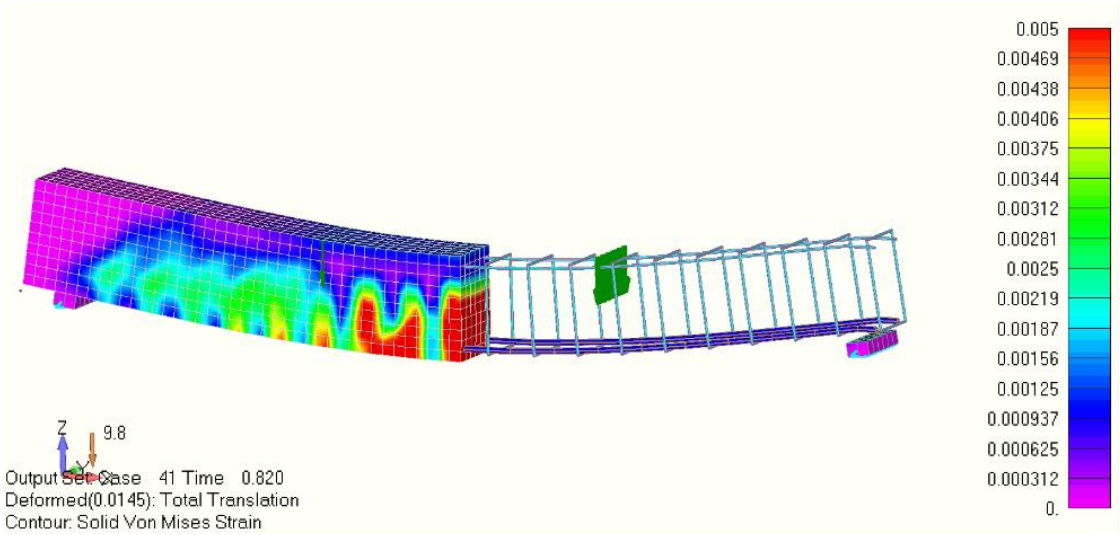

Figure 25. RC beam. Von Mises strain contour and deformed shape prior to failure. 50 load increments.

It is evident that the model manages to capture the experimental data without any numerical instabilities, where the only drawback was the required computational time for the solution due to the large number of elements that were used to discretize the concrete domain. The solution and output writing required around three and a half hours (3.7 GHz processing unit) for the solution of the 50 load increment model. This was also the reason why the main research objective of [32] was to develop a methodology that will use the 3D detailed modeling approach in simulating full-scale RC structures. Nevertheless, the use of the developed modeling approach [2] is not affected more than other existing numerical methods do when the size of the FEs that are used to discretize the concrete domain is changed from larger elements to smaller and vice-versa. On the contrary, the developed method [2] has the ability to provide with objective and accurate results when larger in size finite elements are used, which constitutes this method an ideal modeling approach when dealing with full-scale RC structures.

As a final investigation stage on the ability of the under study modeling approach to capture the mechanical behaviour of the RC beam, a model that assumes a hexahedral mesh size of 10 mm was developed, as it can be seen in Fig. 26.

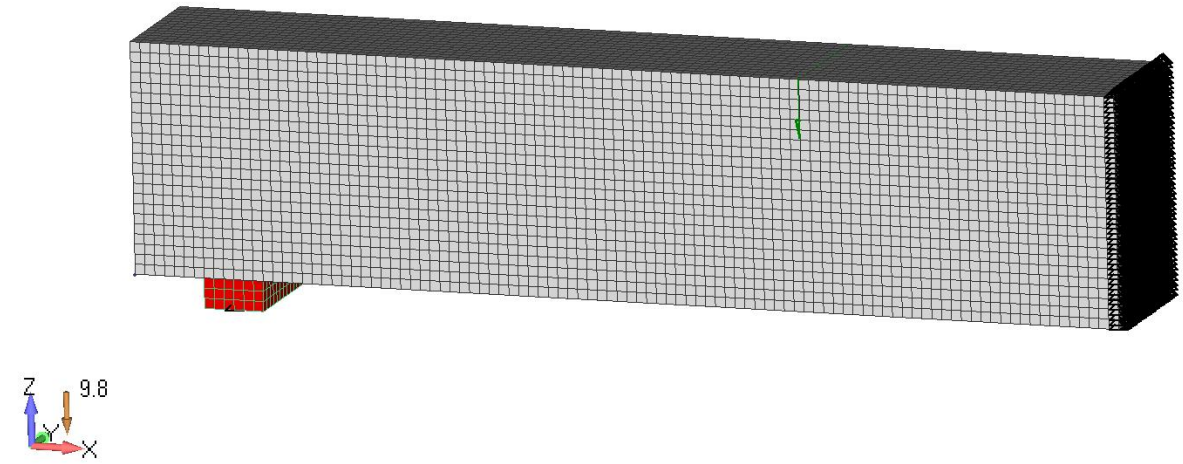

Figure 26. RC beam. Hexahedral element mesh. Model with 10 mm hexahedral edge size.

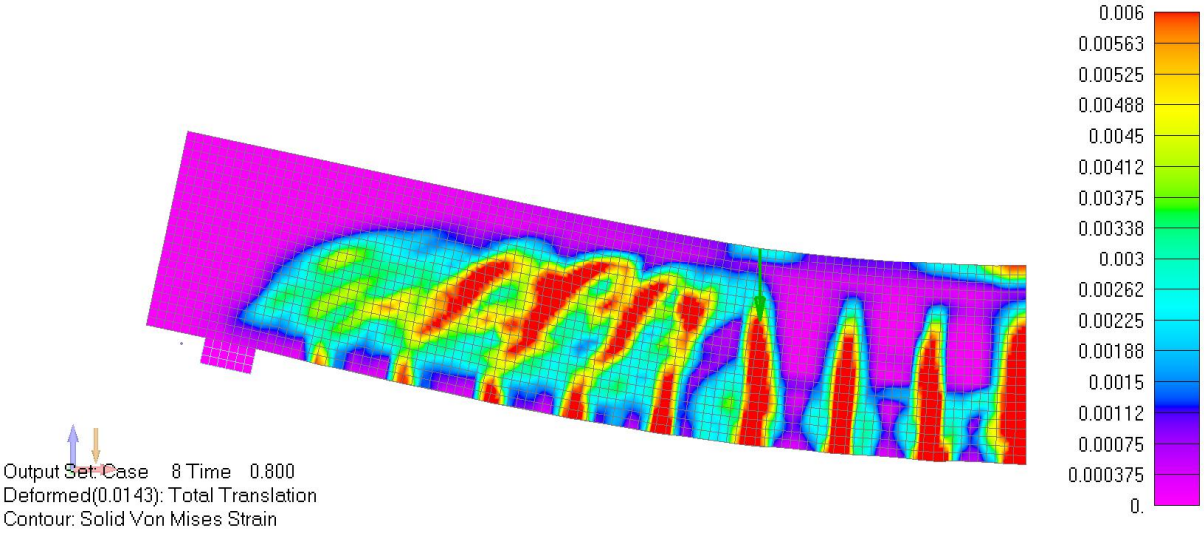

Figure 27. RC beam. Deformed shape and von Mises strain contour prior to failure. Model with 10 mm hexahedral edge size.

The numerical model consists of 34,500 concrete hexahedral elements, where it is easy to observe that only half of the beam was modelled to decrease the computational demand required for the nonlinear analysis. Additionally, the applied load was imposed through 10 load increments, whereas the energy convergence tolerance was set to 10^{-4}. According to the performed nonlinear analysis, the beam failed at load increment 9, where the numerically obtained deformed shape and von Mises strain contour can be seen in Fig. 27. It is easy to observe that the crack development at the midspan and closer to the support are distinctive, highlighting the ability of the numerical method in capturing the crack spacing. Fig. 28 shows the comparison between the experimental results and the two numerical models based on the numerically obtained data, where the 10 mm element size model (ultra-fine) manages to

capture the maximum capacity with the same accuracy but exhibits a more flexible behaviour due to the very fine mesh.

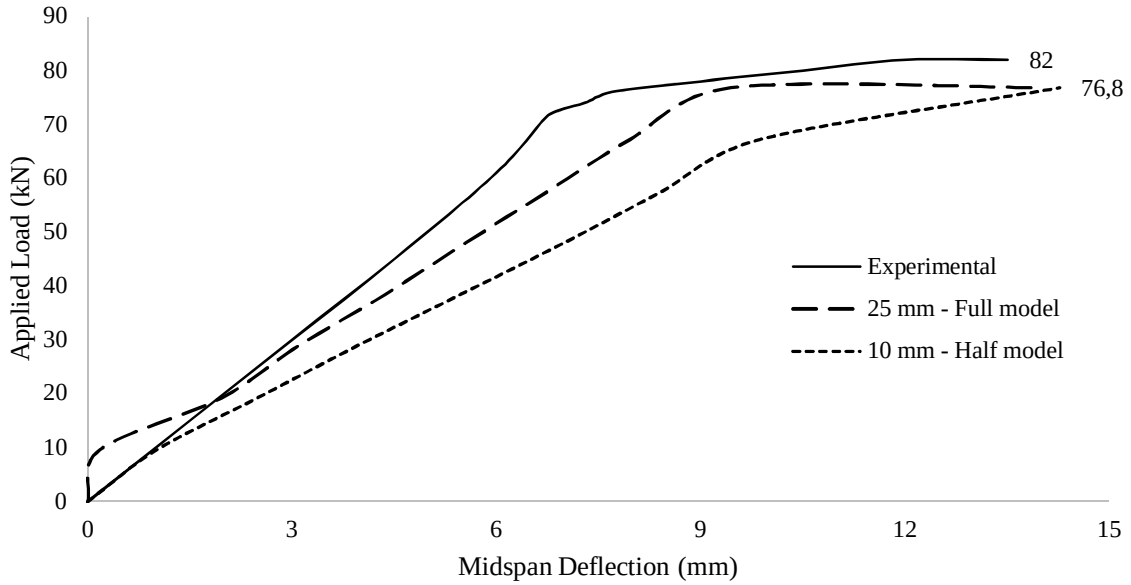

Figure 28. RC beam. Experimental vs 25 mm vs 10 mm element models. P-δ curves.

Conclusively, it is easy to say that the use of fine (25 mm) or even ultra-fine (10 mm) meshes affects the final results like any other model, where the smaller the finite element used discretize the concrete domain the more flexible the mechanical behaviour of the numerical model. In addition to that, it is noteworthy to state that the ultra-fine model developed cracks at the first load increment given that the concrete domain was discretized with a very small element size that was able to capture hairline cracks at the middle of the RC beam. This was also the reason why the mechanical behaviour predicted by the ultra-fine model was more flexible throughout the nonlinear analysis compared to the first model. Furthermore, it is important to say here that the analysis required around 1 week for the case of the ultra-fine model, illustrating the reason why using this discretization approach was not considered in [5] and why the ability to model and analyze RC structures through larger in size hexahedral elements is of significant importance.

Finally, it is also important to note at this point that when a crack opening occurs at a Gauss Point, the failure surface is reached, where the smeared cracking takes place. In the case where the hexahedral finite element has a smaller size then it can be affected by the fact that the larger physical width of the fracture process zone. This can lead to an overestimated fracture work in the simulation deriving a more flexible behaviour. Furthermore, the use of larger load increments may have affected the overall computed numerical response of the beam. Fig. 28 clearly demonstrates an over-flexibility of the specimens that possibly can be attributed to any of these numerical issues. Nevertheless, the model is found to be able to capture the ultimate failure of the RC beam specimen with a 6.3% accuracy in favor of safety.

5. Conclusions

Finite element modelling of plain concrete specimens and a RC beam was performed through the use of the Kotsovos and Pavlovic [1] material model as it was extended by Markou and Papadrakakis [2]. The analyses that were performed foresaw the use of fine meshes in an attempt to investigate a long-time misconception which states that this material model cannot be successfully used when the concrete domain is discretized with elements smaller than 10-20 cm; the specimen sizes of the concrete cylinders tested during the experimental campaign that provided with the data used for the development of the 3D concrete material model [1].

The parametric investigation with fine meshes presented herein that foresaw the construction and analysis of numerous models using the algorithm presented in [2], foresaw the use of experimental data on plain normal strength concrete specimens found in the international literature and experimental data on HSC cylindrical specimens that were obtained by laboratory tests performed by the authors for the needs of this research work. In addition to that, a RC beam that was tested in [39] was used to validate the ability of the FE algorithm proposed in [2] and its ability to reproduce experimental data when fine meshes are used.

According to the numerical findings that were presented in Section 4 of this manuscript, the modeling approach was found to respond satisfactorily for both plain and reinforced concrete specimens. The numerical results provide sufficient evidence in supporting the conclusion that through fine meshes (1-3 cm hexahedral FEs) the modeling approach manages to predict the ultimate strength of uniaxially stressed normal strength concrete specimens with a 5% deviation from the experimental data. The mesh sensitivity analysis showed that the results were not significantly affected. Furthermore, the findings indicated a corresponding 7.5% average difference from the experimental results when the modeling approach was used to analyse the 4 different HSC cylinder groups that were experimentally tested for the needs of this research work.

Finally, the numerical results of a 4-point bending test performed on a 2 m long RC beam fully reinforced with conventional steel rebars demonstrate the ability of the method to capture the experimental results. Different load increment sizes during the nonlinear analyses were also investigated demonstrating the stability and robustness of the nonlinear solution algorithm incorporated in Reconan FEA. Based on the numerical findings, the modeling approach analysed the RC beam by assuming a 25 and 10 mm in size 20-noded hexahedral elements, where the ultimate failure load was captured with a 4.4% average deviation from the experimental data reported in [39].

It is safe to conclude at this point that the numerical investigation performed and presented in this manuscript offer a clear indication that the Kotsovos and Pavlovic material model can be used with both coarse and fine meshes to model the mechanical behaviour of normal or high strength concrete structural members (plain or reinforced). It is also important to note herein that, this is not an attribute that characterises most of the currently available 3D constitutive

material models for concrete that usually require finer meshes so as to provide with a numerically stable solution. Conclusively, the mesh size misconception is not valid in this case, thus the authors strongly believe that this research work is a proof that the under study material model performs numerically well when combined with the finite element method and in a similar manner with any other constitutive material model currently available in the international literature. With the only difference, that it outperforms them when used with coarser meshes [2-26].

Acknowledgements

The numerical modelling and analysis were performed through the use of a fast PC that was purchased under the external financial support received from the Research Development Programme (RDP), year 2019, round No 1, University of Pretoria, under the project titled Future of Reinforced Concrete Analysis (FU.RE.CON.AN.); a research fund awarded to the first author in support to his research activities. This financial support is highly acknowledged. The authors would also like to acknowledge all the hard work and assistance of the laboratory technicians of the Civil Engineering Department of the University of Pretoria, during the experimental campaign that was performed during this research work. Their hard work and support is highly acknowledged.

References

[1] Kotsovos, M.D. and Pavlovic, M.N. (1995), *Structural concrete. Finite Element Analysis for Limit State Design*, Thomas Telford, London.

[2] Markou, G. and Papadrakakis, M., "Accurate and Computationally Efficient 3D Finite Element Modeling of RC Structures", Computers & Concrete, 12 (4), pp. 443-498, 2013.

[3] Engen, M., Hendriks, M. A. N., Øverli, J. A., & Åldstedt, E. (2017), "Non-linear finite element analyses applicable for the design of large reinforced concrete structures", European Journal of Environmental and Civil Engineering, pp. 1-23.

[4] Markou, G., R. Sabouni, Suleiman, F. and El-Chouli, R. (2015), "Full-Scale Modeling of the Soil-Structure Interaction Problem Through the use of Hybrid Models (HYMOD)", International Journal of Current Engineering and Technology, 5 (2), pp. 885-892.

[5] Markou, G. (2015), "Computational performance of an embedded reinforcement mesh generation method for large-scale RC simulations", International Journal of Computational Methods, 12(3), 1550019-1:48.

[6] Markou, G. and Papadrakakis, M., "A Simplified and Efficient Hybrid Finite Element Model (HYMOD) for Non-Linear 3D Simulation of RC Structures", Engineering Computations, 32 (5), pp. 1477-1524, 2015.

[7] Mourlas, C., Papadrakakis, M. and Markou, G., "Accurate and Efficient Modeling for the Cyclic Behavior of RC Structural Members", ECCOMAS Congress, VII European

Congress on Computational Methods in Applied Sciences and Engineering, Crete Island, Greece, 5–10 June 2016.

[8] Markou, G., Mourlas, C. and Papadrakakis, M. (2017), "Cyclic Nonlinear Analysis of Large-Scale Finite Element Meshes Through the Use of Hybrid Modeling (HYMOD)", International Journal of Mechanics, 11(2017), pp. 218-225.

[9] Mourlas, C., Papadrakakis, M. and Markou, G. (2017), "A Computationally Efficient Model for the Cyclic Behavior of Reinforced Concrete Structural Members", Engineering Structures, 141, pp. 97–125.

[10] Mourlas, C., Markou, G. and Papadrakakis, M., "3D nonlinear constitutive modeling for dynamic analysis of reinforced concrete structural members", 10th International Conference on Structural Dynamics, EURODYN, 10-13 September 2017, Sapienza Universita di Roma, Roma, Italy.

[11] Mourlas, C., Papadrakakis, M. and Markou, G., "Computationally efficient and accurate modeling of the cyclic behavior of reinforced concrete structural members under ultimate limit state conditions", 6th International Conference on Computational Methods in Structural Dynamics and Earthquake Engineering, 15-17 June 2017, Rhodes Island, Greece.

[12] AlHamaydeh, M., Markou, G. and Saadi, D., "Nonlinear FEA of Soil-Structure-Interaction Effects on RC Shear Wall Structures", 6th International Conference on Computational Methods in Structural Dynamics and Earthquake Engineering, 15-17 June 2017, Rhodes Island, Greece.

[13] Markou, G., Mourlas, C., Bark, H. and Papadrakakis, M. (2018), "Simplified HYMOD Non-Linear Simulations of a Full-Scale Multistory Retrofitted RC Structure that Undergoes Multiple Cyclic Excitations – An infill RC Wall Retrofitting Study", Engineering Structures, 176 (2018), pp. 892–916.

[14] Markou, G., "A Parallel Algorithm for the Embedded Reinforcement Mesh Generation of Large-Scale Reinforced Concrete Models", 9th GRACM International Congress on Computational Mechanics, Chania, Greece, 4-6 June 2018, pp. 211-218.

[15] Markou, G., AlHamaydeh, M. and Saadi, D., "Effects of the Soil-Structure-Interaction Phenomenon on RC Structures with Pile Foundations", 9th GRACM International Congress on Computational Mechanics, Chania, Greece, 4-6 June 2018, pp. 338-345.

[16] Mourlas, C., Markou, G. and Papadrakakis, M., "Accumulated Damage in Nonlinear Cyclic Static and Dynamic Analysis of Reinforced Concrete Structures Through 3D Detailed Modeling", 9th GRACM International Congress on Computational Mechanics, Chania, Greece, 4-6 June 2018, pp. 38-46.

[17] Saadi, D., AlHamaydeh, M. and Markou, G., "Investigation of Soil-Structure-Interaction Effects on RC Shear Wall Structures via Nonlinear FEA", UAEGSRC2018, The Fourth UAE Graduate Students Research Conference, American University of Sharjah, UAE, April 21, 2018.

[18] Markou, G. and Genco, F. (2019), “Seismic Assessment of Small Modular Reactors: NuScale Case Study for the 8.8 Mw Earthquake in Chile”, Nuclear Engineering and Design, 342(2019), pp. 176-204.

[19] Mourlas, C., Markou, G. and Papadrakakis, M. (2019), “Accurate and Computationally Efficient Nonlinear Static and Dynamic Analysis of Reinforced Concrete Structures Considering Damage Factors”, Engineering Structures, 178 (2019), pp. 258–285.

[20] Markou, G., Mourlas, C. and Papadrakakis, M. (2019), “A Hybrid Finite Element Model (HYMOD) for the Non-Linear 3D Cyclic Simulation of RC Structures”, International Journal of Computational Methods, 16(1), 1850125: 1-40.

[21] Mourlas, C., Gravett, D.Z., Markou, G., and Papadrakakis, M., “Investigation of the Soil Structure Interaction Effect on the Dynamic Behavior of Multistorey RC Buildings”, VIII International Conference on Computational Methods for Coupled Problems in Science and Engineering, COUPLED PROBLEMS 2019, 3-5 June 2019, Sitges, Catalonia, Spain.

[22] Markou, G., Mourlas, C., Garcia, R., Pilakoutas, K. and Papadrakakis, M., “Cyclic Nonlinear Modeling of Severely Damaged and Retrofitted Reinforced Concrete Structures”, COMPDYN 2019, 7th International Conference on Computational Methods in Structural Dynamics and Earthquake Engineering, 24-26 June 2019, Crete, Greece.

[23] Gravett, D.Z., Mourlas, C., Markou, G., and Papadrakakis, M., “Numerical Performance of a New Algorithm for Performing Modal Analysis of Full-Scale Reinforced Concrete Structures that are Discretized with the HYMOD Approach”, COMPDYN 2019, 7th International Conference on Computational Methods in Structural Dynamics and Earthquake Engineering, 24-26 June 2019, Crete, Greece.

[24] Mourlas, C., Markou, G., and Papadrakakis, M., “3D Detailed Modeling of Reinforced Concrete Frames Considering accumulated damage during static cyclic and dynamic analysis – new validation case studies”, COMPDYN 2019, 7th International Conference on Computational Methods in Structural Dynamics and Earthquake Engineering, 24-26 June 2019, Crete, Greece.

[25] Markou, G., “Numerical Investigation of a 3D Detailed Limit-State Simulation of a Full-Scale RC Bridge”, SEECCM III, 3rd South-East European Conference on Computational Mechanics, Kos Island, Greece, 12–14 June 2013.

[26] Markou, G. and AlHamaydeh, M. (2018), “3D Finite Element Modeling of GFRP-Reinforced Concrete Deep Beams without Shear Reinforcement”, International Journal of Computational Methods, 15(1), pp. 1-35.

[27] Abaqus Analysis User’s Manual 6.12 (2019), Dassault Syst`emes Simulia Corp., Providence, RI, USA.

[28] LS-DYNA. LS-DYNA. (2019), User manual, Livermore Software Technology Corporation. www.ls-dyna.com.

[29] ANSYS structural, (2019), https://www.ansys.com

[30] Cotsovos D. M., Zeris Ch. A. and Abas A. A., “Finite element modeling of structural concrete,” ECCOMAS thematic Conf. comput. Methods Struct. Dyn. Earthq. Eng., COMPDYN 22–24 June, 2009, Rhodes, Greece.

[31] Abed, F. H., Abdullah, Al-R. and Al-Rahmani, A. H. (2013), “Finite element simulations of the shear capacity of GFRP-reinforced concrete short beams,” IEEE 5th Int. Conf. Simul. Appl. Optim. (ICMSAO), pp. 1–5.

[32] Markou, G., (2011), Detailed Three-Dimensional Nonlinear Hybrid Simulation for the Analysis of Large-Scale Reinforced Concrete Structures, Ph.D. Thesis, NTUA.

[33] EN1992-1-1, Eurocode 2 (2004), Design of concrete structures.

[34] SANS 50197-01, 2013. Cement, Part 1: Composition, specifications and conformity criteria for common cements, South African National Standard.

[35] Willam K. J. and Warnke E. P., (1974), “Constitutive model for the triaxial behaviour of concrete”, Seminar on concrete structures subjected to triaxial stresses, Instituto Sperimentale Modeli e Strutture, Bergamo, Paper III-1.

[36] ReConAn v1.00 Finite Element Analysis Software User's Manual, 2010.

[37] Menegotto M., and Pinto P. E. (1973), “Method of analysis for cyclically loaded reinforced concrete plane frames including changes in geometry and non-elastic behavior of elements under combined normal force and bending”, Proceedings, IABSE Symposium on Resistance and Ultimate Deformability of Structures Acted on by Well Defined Repeated Loads, Lisbon, Portugal, 15–22.

[38] Kim N.-S., Lee J.-H. and Chang S.-P. (2009), “Equivalent multi-phase similitude law for pseudodynamic test on small scale reinforced concrete models”, Engineering Structures Vol. 31, pp. 834-846.

[39] Kearsley, E. and Jacobsz, SW, “Condition assessment of reinforced concrete beams – Comparing digital image analysis with optic fibre Bragg gratings”, ICCRRR 2018, MATEC Web of Conferences 199, 06011 (2018).

[40] Lykidis G. (2007), “Static and Dynamic Analysis of Reinforced Concrete structures with 3D Finite Elements and the smeared crack approach”, Ph.D. Thesis, NTUA, Greece, 2007.

[41] Spiliopoulos K.V. and Lykidis G.Ch. (2006), “An efficient three-dimensional solid finite element dynamic analysis of reinforced concrete structures”, Earthquake Engng Struct. Dyn., Vol. 35, pp. 137-157.

[42] Wells, G. N., & Sluys, L. J. (2001). A new method for modelling cohesive cracks using finite elements. International Journal for Numerical Methods in Engineering, 50(12), 2667-2682.

[43] Li, X., & Chen, J. (2017). An extended cohesive damage model for simulating arbitrary damage propagation in engineering materials. Computer Methods in Applied Mechanics and Engineering, 315, 744-759.

[44] Li, X., Gao, W., & Liu, W. (2019). A mesh objective continuum damage model for quasi-brittle crack modelling and finite element implementation. International Journal of Damage Mechanics, 28(9), 1299- 1322.